Visual Neuroscience (1997), **14**, 1129–1142. Printed in the USA.

Differential timing for the appearance of neuronal and astrocytic β-adrenergic receptors in the developing rat visual cortex as revealed by light and electron-microscopic immunocytochemistry

CHIYE AOKI

Center for Neural Science and Biology, New York University, New York

(RECEIVED February 26, 1997; ACCEPTED May 30, 1997)

Abstract

The developing cerebral cortex is likely to exhibit synaptic circuitries differing from those in adulthood, due to the asynchronous maturation of the various neurotransmitter systems. Two antisera directed against mammalian β-adrenergic receptors (βAR), βAR248 and βAR404, were used to characterize the laminar, cellular, and subcellular distributions of βAR in postnatally developing visual cortex of rats. The antigenic sites were the receptor's third intracellular loop for βAR248 and the C-terminus for βAR404. During week 1, most of the βAR404- and βAR248-immunoreactive sites were dendritic. Morphologically identifiable synapses were rare, even in layer 1: yet, semiquantitative analysis revealed that βAR404-immunoreactive synapses comprise half of those in layer 1. During week 2, the two antisera began to diverge in their immunoreactivity patterns. With βAR248, there was an overall decline in immunoreactivity, while with βAR404, there was an increase in immunoreactive sites, primarily due to labeled astrocytic processes that increased 200-fold in areal density by week 3. In contrast, the areal density of synaptic labeling by βAR404 barely doubled, in spite of the 30-fold increase in areal density of synapses. These results suggest that βAR undergo conformational changes during early postnatal periods, causing alterations in their relative antigenicity to the two antisera. Furthermore, the first 2 weeks appear to be characterized by modulation of earliest-formed synapses, and the subsequent phase is marked by addition of astrocytic responses that would be more diffuse temporally and spatially. Activation of βAR is recognized to increase visually evoked activity relative to spontaneous activity. Moreover, astrocytic βAR are documented to regulate extracellular concentrations of glutamate, ATP, and neurotrophic factors important for the formation of binocular connections. Thus, neuronal and astrocytic responses may, together and in tandem, facilitate strengthening of intracortical synaptic circuitry during early life.

Keywords: Synaptogenesis, Ultrastructure, Immunoelectron microscopy, Norepinephrine, Neuromodulation, Presynaptic

Introduction

Although it is recognized that nearly all of the morphologically identifiable synapses in the adult visual cortex are formed after birth (Cragg, 1975; Blue & Parnavelas, 1983*a*,*b*), relatively little is known about the emergence of chemically identified synapses during postnatal development. Noradrenergic axons enter the cortical mantle prenatally and prior to the entry of thalamic afferents (Coyle & Molliver, 1977; Levitt & Moore, 1979). Thus, these axons are in place to form some of the very first cortical synapses (Molliver & Kristt, 1975). An idea has been put forth that noradrenaline, together with acetylcholine, may have a role during development that is distinct from that in adulthood—namely, to support the formation of excitatory and inhibitory synapses in cortex—and that this process yields receptive-field properties mirroring early postnatal experience (Bear & Singer 1986; Gordon et al., 1990; Kasamatsu, 1991). However, while results obtained from receptor autoradiography indicate that lesion of thalamic sensory afferents can cause decrease of β-adrenergic receptor (βAR) density in the visual cortex (Vos et al., 1990; Liu et al., 1993), visual deprivation during the critical period for ocular dominance plasticity has little effect on the laminar distribution of βAR there (Wilkinson et al., 1983; Aoki et al., 1986). Moreover, the adult pattern of βAR distribution across the layers of the visual cortex appears to be established prior to the onset of critical period (Aoki et al., 1986). These findings suggest that developmental plasticity is dependent on a biochemical event distal to βAR activation, rather than alteration of βAR expression itself. Alternatively, receptor autoradiog-

Reprint requests to: Chiye Aoki, Center for Neural Science, New York University, 6 Washington Place, Rm 809, New York, NY 10003, USA.

raphy could fail to detect some developmental changes, such as in the cellular and subcellular distribution of receptors or the insertion of receptors at newly formed synapses that occur during the critical period and/or in response to visual deprivation. Thus, electron-microscopic immunocytochemistry was used to determine the following: (1) How early βAR-modulated synapses form; and (2) Whether nascent and mature noradrenergic synapses exhibit classic morphological signatures. The second issue was prompted by the observation that noradrenergic fibers in adult cortex rarely form morphologically identifiable synaptic junctions (Descarries et al., 1977; Séguéla et al., 1990) and that mature dendrites display α2- and βAR at nonjunctional sites (Aoki, 1992; Venkatesan et al., 1996). These data suggest a nonjunctional modulation by noradrenaline. To determine whether the neonatal cortex also exhibits these characteristics, we used two antisera generated against mammalian βAR (hamster lung, β2-type) to determine the receptor's cellular and subcellular localization within developing visual cortices of rats. The antisera recognize both the β1- and β2-subtypes (Strader et al., 1987*a*,*b*). Earlier observations indicated that the antiserum, βAR404, directed against the C-terminus of βAR, recognizes astrocytes, predominantly, in the adult cerebral cortex (Aoki, 1992) and other brain regions (Aoki & Pickel, 1992), but neuronal processes in neonatal cortices (Aoki & Venkatesan, 1994). To examine this phenomenon more closely, semiquantitative survey of βAR404-immunoreactivity (ir) also was carried out and the following questions were asked: (1) What are the areal densities of βAR404-ir in neuronal and glial processes at varying postnatal ages? (2) What portion of neuronal βAR404-ir occur at morphologically identifiable synaptic junctions? (3) What portion of βAR404-ir occur postsynaptically versus presynaptically? The analysis was performed upon layer 1 or its embryonic anlage, the marginal zone, since this layer contains the highest density of noradrenergic fibers (Morrison et al., 1978) and βAR (Schliebs & Godicke, 1988) in adulthood.

Methods

Source of immunoreagents

Antisera directed against βAR were generous gifts from Dr. C. D. Strader of Merck Sharp and Dohme Research Laboratories (Rahway, NJ). These antisera were generated using synthetic peptides corresponding to amino acids 248–254 and 404–418 of hamster lung (β2-type) adrenergic receptors (Dixon et al., 1986). Here, they will be referred to as βAR248 and βAR404, respectively. The specificity of βAR404 and βAR248 for βAR was demonstrated earlier using the Western blot method and showing that cell lines transfected with mutants deleted in the C-terminus are not immunoreactive for βAR404 (Strader et al., 1987*b*). Specificity of antisera also was demonstrated by immunoprecipitation of ^{125}I-cyanopindolol-radiolabeled βAR (Strader et al., 1987*a*). Further studies on their specificity was performed in the current study, as summarized below under "Control." Biotinylated goat-anti-rabbit IgG and the avidin-biotinylated peroxidase complex were purchased from Vector (Burlingame, CA) as the Vector Elite Kit.

Preparation of brain tissue

Earlier studies indicated that the addition of acrolein to the fixative greatly enhances preservation of the ultrastructure without diminishing βAR antigenicity (Aoki et al., 1987; Aoki, 1992). Thus, visual cortical sections of varying ages were prepared from brains transcardially fixed with a mixture of acrolein and paraformaldehyde. Six adult rats and three litters of neonatal rats (n = 35) were used. The age of neonatal rats ranged from postnatal day (PND) 0 (= birthday) to 30, at which time ultrastructural features are reported to be nearly indistinguishable from those of adults (Blue & Parnavelas, 1983*a*,*b*). Two were perfused at PND 0, 12 at PND 2–4, six at PND 6–7, six at PND 9–10, four at PND 13/14, two at PND 18, two at PND 24, and one at PND 30. All rats were anesthetized using Nembutal (50 mg/kg bodyweight). Upon confirmation that they did not respond to light tactile stimulation of the cornea, these animals were rapidly perfused through the ascending aorta or left ventricle with the following solutions using a peristaltic pump: (1) heparinized saline, maintained at pH 7.4 using 0.01 M phosphate buffer (PB), for about 1 min; then (2) 50 ml of an aldehyde mixture consisting of 3% acrolein and 4% freshly prepared paraformaldehyde, buffered to pH 7.4 using 0.1 M PB; followed by (3) 4% paraformaldehyde alone, buffered with 0.1 M PB. Adults were perfused at a rate of 70 ml/min. Neonates were perfused at slower rates ranging from 15 to 50 ml/min. Adult rat brains were sectioned on the same day using a Vibratome at a thickness of 40 μm. Neonatal tissue were postfixed overnight at room temperature in perfusate (3), then sectioned at a thickness ranging from 60 to 100 μm. Sections were immersed in a solution containing 1% sodium borohydride in 0.1 M PB to terminate further cross-linking of proteins by the aldehydes (King et al., 1983). After rinsing in 0.1 M PB, these sections were rinsed in 0.1 M Tris-buffered saline (TBS) adjusted to pH 7.6 using HCl.

Light-microscopic immunocytochemistry

The avidin-biotinylated peroxidase complex method of Hsu (1981) was used to visualize immunoreactive sites. Previous studies using adult tissue had shown that a dilution ranging from 1:1000 to 1:2000 for the primary antiserum and an incubation time of *ca.* 18 h at room temperature was optimal for differentiating background labeling from specific labeling to reach antigenic sites (Aoki, 1992). This protocol was followed for the series of experiments presented here. It was also shown previously that the addition of permeabilizing agents, such as Triton X-100, was not necessary for these antisera (Aoki, 1992). Thus, all incubation solutions in this study were without membrane-permeabilizing agents. Sections were mounted on gelatin-coated slides and examined using an Olympus light microscope.

Electron-microscopic immunocytochemistry

Sections processed for immunocytochemistry were postfixed by immersing them for 10 min at room temperature in saline containing 2% glutaraldehyde and buffered with 0.1 M PB. Fixation was terminated by rinsing sections repeatedly in saline (0.9% sodium chloride) buffered with 0.01 M PB. All sections were further postfixed for 1 h with 2% osmium tetroxide buffered by 0.1 M PB, then rinsed in 0.1 M PB. Prior to infiltration in the resin, EMBED 812 (EMS), sections were immersed in 70% ethanol containing 2% uranyl acetate for 1 h or overnight, then dehydrated further using 90% and 100% ethanol. Following two immersions in 100% acetone for 10 min each, sections were transferred into a mixture consisting of 50% acetone and 50% EMBED 812. This was followed by an incubation in 100% EMBED 812 resin for 2 h or overnight. Sections then were flat-embedded between two sheets of Aclar plastic and cured overnight in an oven set to 60°C. Subsequently, regions containing all layers of area 17 of the visual

https://doi.org/10.1017/S0952523800011822 Published online by Cambridge University Press

cortex were re-embedded in Beem capsules, and sectioned at thicknesses ranging from 70 to 100 nm. Some of the ultrathin sections were counterstained with lead citrate to facilitate visualization of details while others were left unstained in order to optimize detection of immunoperoxidase labels over electron-dense organelles, such as postsynaptic densities.

Control immunocytochemical staining procedures

To determine whether the immunostaining pattern was specific, some sections were incubated with a 1:2000 dilution of the antisera that had been preadsorbed. The preadsorption was achieved by incubating 2.5 ml of the antisera, diluted to 1:2000, with 3 mg of synthetic peptides for 18 h at room temperature. The peptides contained a sequence with exact correspondence to the antigens used for generating the respective rabbit polyclonal antisera. Specifically, the peptides corresponded to the third intracellular loop portion (residues 247–258 of hamster lung βAR; H-QVEQDGR SGHGL-OH) and C-terminus (residues 404–418; H-CLDSQGRN3 STNDSPL-OH where 3 = norleucine). These peptides were custom-made by Research Genetics, Inc. (Huntsville, AL).

Semiquantitative analysis of ultrathin sections

Analysis of βAR404-ir sites was performed upon layer 1 (marginal zone) of various ages to determine the areal density of immunolabeled dendritic shafts, dendritic spines, axons, and astrocytes. For each dendritic and axonal profile, the presence or absence of morphologically identifiable synapse was noted. Furthermore, the areal density of all morphologically identifiable synaptic junctions, whether or not labeled, was determined. The data were collected strictly from portions of the ultrathin sections exhibiting tissue-resin interface. To determine the area of the analyzed region, a low-magnification electron micrograph (750×) of the surveyed grid square was taken. Using a digitizing software (NIH Image), the surveyed neuropil area was measured, excluding portions occupied by blood vessels (including the basal lamina), nuclei, and pure resin. These analyses should be considered semiquantitative, rather than quantitative, because age-dependent and interanimal variabilities in tissue fixation and efficiency of immunoreactivity could not be assessed quantitatively. However, interexperiment variabilities were minimized by processing tissue of different ages in equivalent incubation buffers.

Results

Identification of the emerging laminar boundaries within neonatal visual cortex was greatly facilitated by using near-adjacent Nissl- and cytochrome oxidase-stained reference sections. In earlier studies on the developing rat visual cortex, Kageyama and Robertson (1993) and Aoki et al. (1994) used the terms, "marginal zone," for future layer 1 and "cortical plate" for future layers 2–4 at PND 0–2 and layers 2–3 at PND 4. This report follows that terminology.

Light microscopy revealed that the immunocytochemical staining patterns with both βAR248 and βAR404 resembled the Nissl staining pattern during the first week, indicating that neuronal perikarya were the predominant immunoreactive elements for the two antisera. During the second week, βAR248-ir weakened progressively while βAR404-ir persisted but switched from predominantly neuronal to predominantly astrocytic sites.

Laminar distribution of βAR248-ir

Application of the antiserum directed against the third intracellular loop, βAR248, resulted in robust labeling of neurons as early as PND 0 (not shown). Throughout the layers, the immunolabeling was mainly in a thin ring of somatic cytoplasm. There was no apparent dendritic labeling. By PND 4, the neuronal cell bodies in layer 6b (Fig. 1C), as well as those in layer 5 (Fig. 1A), attained greater immunoreactivity and were of distinctly larger diameter than those in layer 4 (Fig. 1B). Apical dendrites associated with neurons of layer 6 also were intensely immunoreactive. In contrast, neurons in the upper strata of cortical plate showed weaker perikaryal labeling and virtually no dendritic labeling (Figs. 1A and 1B), as seen at PND 0.

During the following week, change was most notable in the supragranular layers (referred to as the cortical plate at earlier stages). This zone, which showed only ill-defined immunoreactivity at PND 4, began to exhibit immunolabeled neuronal perikarya and proximal dendrites, including apical dendrites (Figs. 2A and 2B). Strong immunoreactivity persisted in layer 6b, where perikarya began to exhibit adult-like fusiform morphology and immunoreactivity in the basal dendrites (Fig. 2C). Apical dendrites as well as perikarya of pyramidal neurons in layers 5 (Fig. 2A) and 6a (Fig. 2C) continued to exhibit prominent immunoreactivity (Fig. 2C), while neuropil labeling in layer 1 declined (Figs. 2A and 2B).

Beyond the second week, perikaryal and dendritic labeling declined precipitously (not shown). Neuropil labeling appeared homogeneous, as seen in adulthood (Aoki, 1992). Attempts to enhance immunolabeling by extending primary antisera incubation or the peroxidase reaction durations resulted in diffuse perikaryal labeling without any resolvable labeling of dendrites or of finer processes. Increases in primary antibody concentration enhanced nonspecific labeling, only.

Subcellular distribution of βAR248-ir

Electron microscopy revealed that, at PND 4, many of the immunoreactive dendrites exhibit irregular contours and lack identifiable cytoskeleton, indicating that these are growth cones (Fig. 3). Smooth saccules within dendritic growth cones were immunoreactive (Fig. 3B) as were portions of the plasma membrane lacking identifiable synaptic specialization (Fig. 3A). Some of the dendritic processes appeared to surround axon terminals, suggesting that these dendrites are more malleable than the axons' extending tips (Fig. 3A). The immunoreactive postsynaptic densities were of the thick type, similar to Gray's type 1 asymmetric excitatory synapses (Gray, 1959).

The precipitous, global decrease in immunoreactivity by the third postnatal week, as seen by light microscopy, correlated with increasingly confined subcellular distributions of immunoreactivity. Typically, immunoreactivity occurred within small spines (<0.5 μm in diameter) (Fig. 3C). Within such immunoreactive spines, labeling was concentrated over postsynaptic densities, although not strictly confined to these sites (Fig. 3C). By PND 14, immunolabeling was also detectable within axons (not shown) and along astrocytic plasma membranes (Fig. 3D).

Laminar distribution of βAR404-ir

At the earliest age examined, i.e. PND 0–2, immunoreactivity was most robust in the white matter and future layer 1, i.e. the marginal zone (Fig. 4). In the white matter, immunoreactivity was apparent

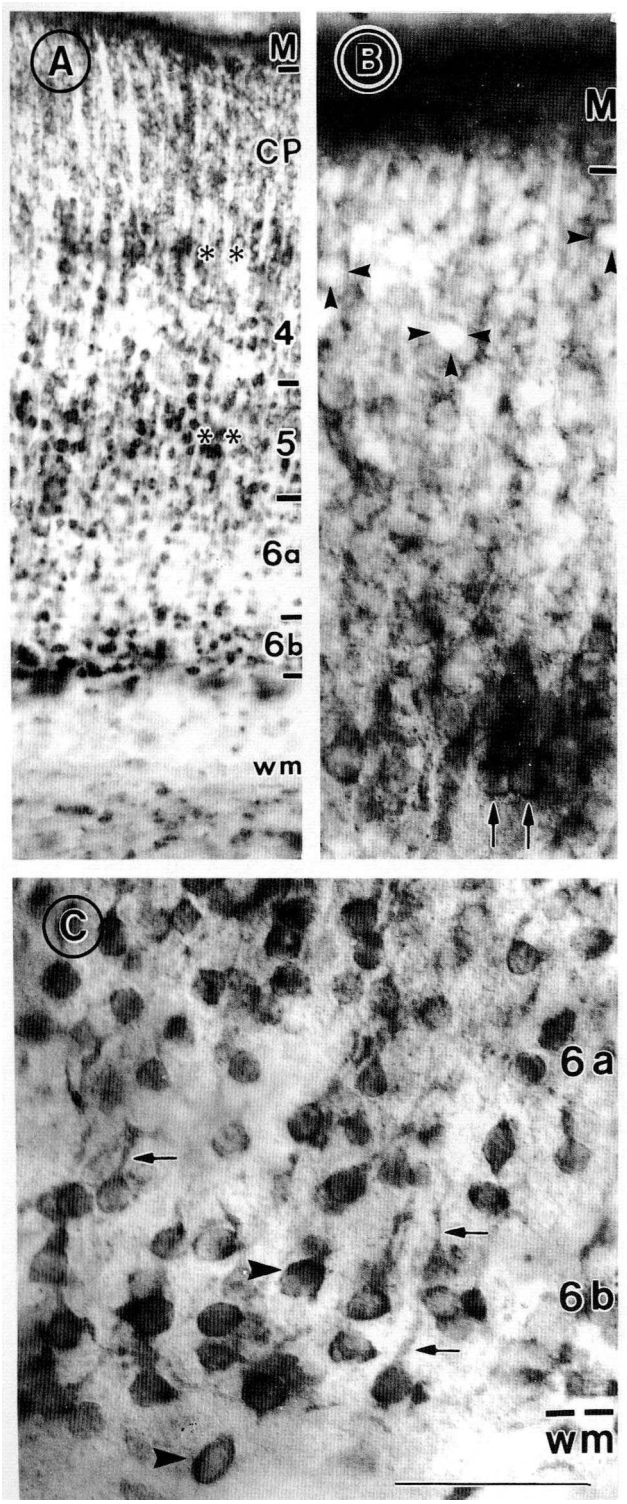

Fig. 1. Light micrographs depicting the laminar distribution of βAR248-ir at PND 4. A: Immunoreactivity is particularly intense in the marginal zone (M) and where marked by asterisks, in layers 4 and 5 as well as 6b. B: Higher magnification shows small unlabeled perikarya in the most superficial tier of the cortical plate (arrowheads) and intensely immunoreactive perikaryal cytoplasm below (arrows at the bottom). C: In the deepest layers, immunoreactivity is intense within perikarya of pyramidal neurons (arrowhead) as well as their apical dendrites (small arrows). wm: white matter. Scale bar = 200 μm in A, 50 μm in B and C.

within many perikarya that were devoid of immunoreactive processes (Fig. 4C). Within the marginal zone, immunoreactivity consisted of a dense collection of small puncta, barely resolvable even with the aid of Nomarski-differential interference contrast (Fig. 4B). Just below the marginal zone, immunoreactivity was concentrated over short processes of unidentifiable origins (Fig. 4B).

The diffuse immunoreactivity that spanned the cortical plate at PND 2 showed remarkable changes during the next 2 days. By PND 4, the base of the cortical plate began to exhibit distinctly immunoreactive dendrites arising from the apex of neuronal perikarya residing in layer 4 (Figs. 5A and 5C). Immunoreactivity within these apical dendrites could be followed into the cortical plate above layer 4 (Fig. 5A). Small immunoreactive puncta persisted in the marginal zone (Fig. 5B) and in layer 6B (Fig. 5A). In addition, the transition zone between the marginal zone and the cortical plate exhibited intense immunoreactivity (Fig. 5B). In the white matter, the perikarya began to exhibit more prominent processes. These processes appeared to reach towards processes extending from neighboring immunoreactive perikarya (Fig. 5D).

During the second postnatal week, βAR404-ir intensified throughout the cortical layers. Immunoreactivity within all of the layers consisted of clustered puncta in the neuropil (Fig. 6A). Immunoreactivity within perikarya was relatively less intense (Fig. 6B). In addition, immunoreactivity in layer 6a consisted of thick processes pointing towards pial surfaces (not shown), while those in layer 6b consisted of radiating processes emerging from small perikarya, most likely of astrocytes (Fig. 6B). This pattern of immunolabeling persisted beyond the second postnatal week.

Subcellular distribution of βAR404-ir

Ultrastructural examination of immunoreactive puncta in the marginal zone of PND 4 tissue revealed that these reflect discrete clusters of immunoreactivity along the plasma membrane of dendrites. Most of these were apparently nonsynaptic clusters within dendritic growth cones (Fig. 7A), while others reflected concentration of immunoreactivity over postsynaptic densities and nearby saccules (Fig. 7B). Immunoreactivity also occurred diffusely within elongated processes which could not be identified as axonal, dendritic, or astrocytic (Figs. 7B).

In the cortical plate, perikarya occurred closely packed against one another, as there were very few dendritic, axonal, or astrocytic processes occupying the neuropil. In this layer, immunoreactivity was largely confined to patches of perikaryal plasma membrane with slight diffusion of the diaminobenzidine (DAB) reaction product into the cytoplasm (Fig. 8). Examination of the white matter by electron microscopy revealed that the immunoreactive perikarya are astrocytic, based on the irregular contour of the plasma membrane and homogeneous distribution of chromatin within nuclei (Peters et al., 1991) (not shown).

Electron-microscopic examination of tissue during the second postnatal week revealed a shift in neuronal perikaryal labeling from plasma membrane to more intracellular domains, such as the Golgi apparatus and smooth endoplasmic reticulum (not shown). The most notable change during the second week was the emergence of immunoreactivity within astrocytic processes (Fig. 9). Astrocytic processes were identified easily by the highly irregular contour, paucity of organelles, and absence of synaptic junctions. Immunoreactivity was enriched along their plasma membranes but was also associated with intracellular saccules.

Immunoreactivity was clearly evident over postsynaptic densities. The dendrites exhibiting immunoreactive postsynaptic densi-

https://doi.org/10.1017/S0952523800011822 Published online by Cambridge University Press

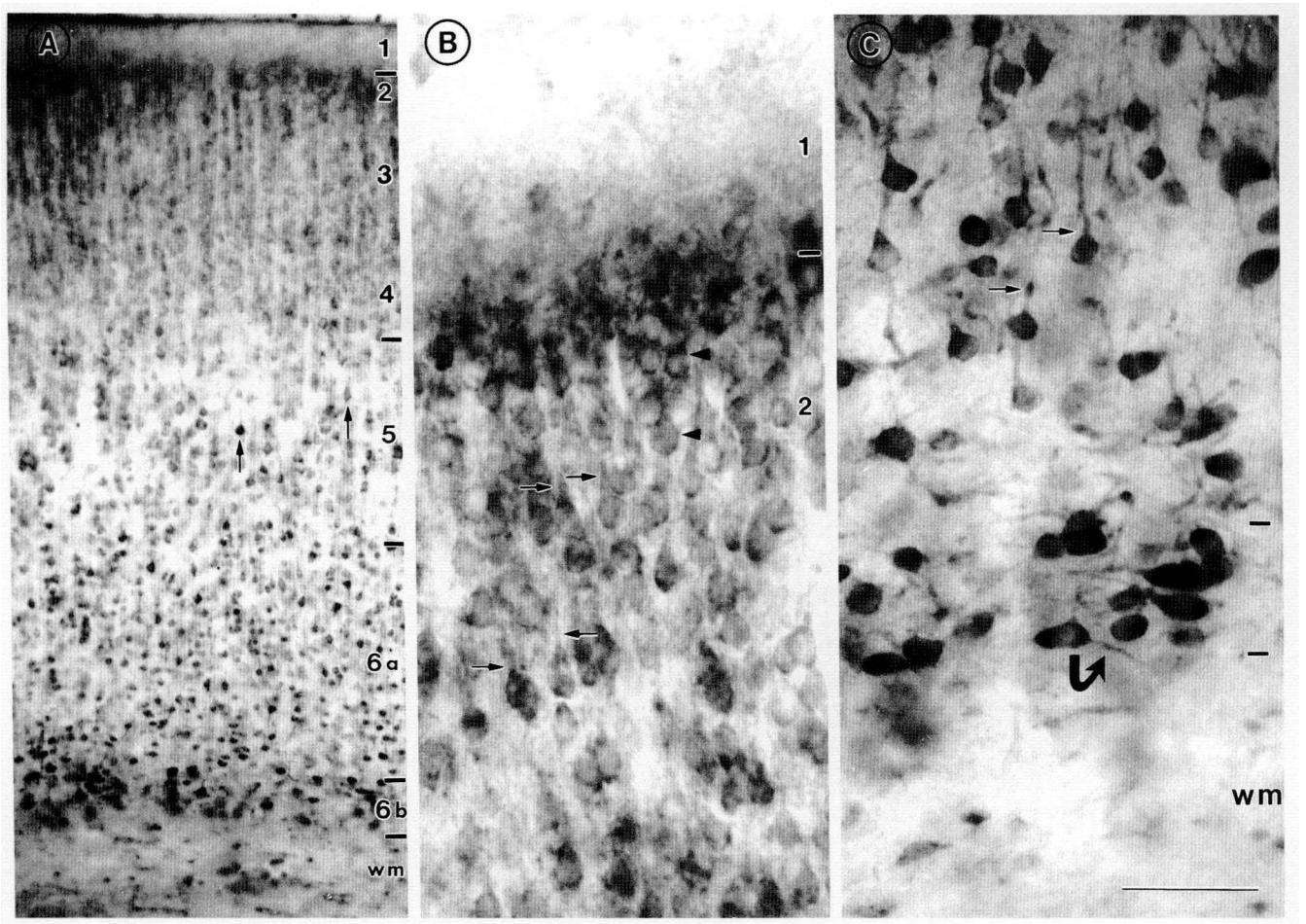

Fig. 2. At PND 9, βAR248-ir is evident in all layers except for 1. A: Arrows point to pyramidal neurons in layer 5 that show immunoreactivity within perikarya as well as their apical dendrites. B: The light micrograph taken at a higher magnification reveals that the less intense immunoreactive profiles in the supragranular layers consist of neuronal perikarya (arrowheads) and their apical dendrites (small arrows). C: Immunoreactivity in layer 6 is clearly identifiable in the neuronal perikarya but excluding the nucleoplasm. Note the labeling in apical dendrites (small arrows) in layer 6a (above the two lines) and in the basal dendrites (curved large arrow) in layer 6b (between the two lines to the right). The white matter (wm) is largely devoid of immunoreactivity. Scale bar = 200 μm in A, 50 μm in B and C.

ties had smooth contours, unlike those seen at PND 4 (compare Figs. 9A with 7B). Immunoreactive spines also emerged by PND 10. As seen in tissue from younger animals, immunoreactivity within dendrites was concentrated over postsynaptic membranes, but these were contiguous with immunoreactivity along extrasynaptic plasma membrane patches and intracellular saccules in the immediate vicinity (Figs. 9A and 9C).

Axonal labeling was first noted at PND 7. By PND 10, both symmetric (Fig. 9B) and asymmetric (not shown) synaptic junctions associated with immunoreactive presynaptic terminals could be discerned. These terminals contained numerous, uniformly small, round vesicles and a small number of dense-cored vesicles (Fig. 9B).

Semiquantitative analysis of layer 1 neuropil (Table 1) indicated that synapses are very sparse during the first week (less than 1 synapse in 2330 μm^2). However, among the few that were present, more than half were immunoreactive for βAR404 (13 of the 20 synapses encountered in 4660 μm^2 of surveyed area). There was no apparent developmental change in the areal density of synaptic labeling beyond postnatal week 1. However, since the areal density of synapses increased more than 30-fold from the first to the third week, the portion of immunoreactive synapses dropped to less than 5 % of all synapses. Also notable was an increase in portion of dendritic labeling occurring over synapses: these increased from two thirds in week 1 to nearly all by week 3. The presynaptic versus postsynaptic labeling also were changed from 100% postsynaptic at PND 4 to 80% postsynaptic/20% presynaptic at PND 24. Finally, the areal density of astrocytic labeling was altered drastically during the sampled postnatal period, showing an approximately 200-fold increase from PND 4 to PND 24, and nearly 20-fold greater areal density than of synaptic labeling by PND 24.

Results from control experiments

Light-microscopic analysis showed that the areal density of βAR248-ir perikarya, most likely of pyramidal neurons based on their association with proximal dendrites projecting towards pial surface, was reduced by greater than 75%. The few that remained identifiable were close to threshold for immunodetection. Similarly, light-microscopic inspection of βAR404-ir revealed that the

https://doi.org/10.1017/S0952523800011822 Published online by Cambridge University Press

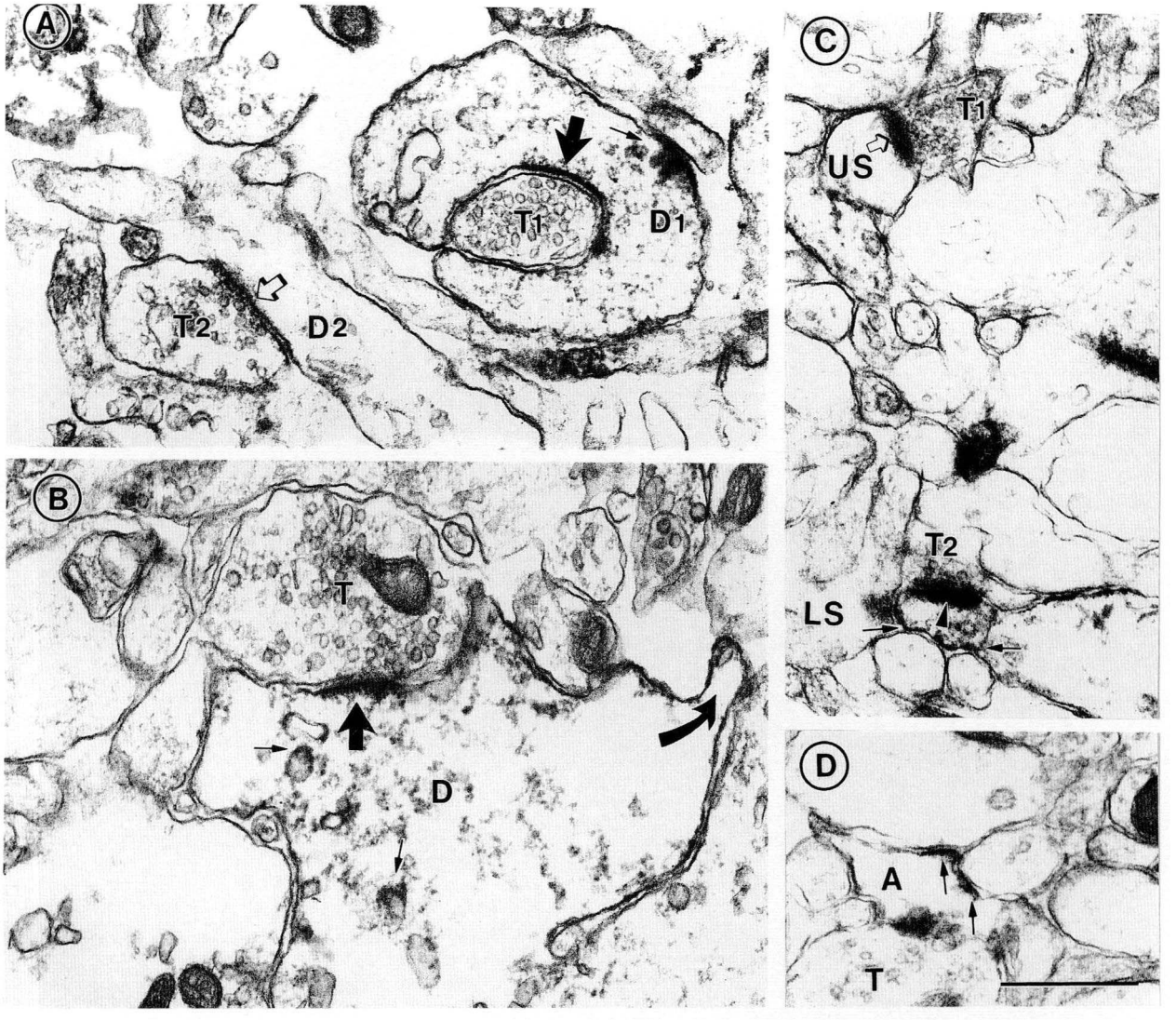

Fig. 3. Electron micrographs showing βAR248-ir in layer 1 at PND 4 and PND 14. A: Two axo-dendritic synapses from PND 4 tissue are shown. One of these synapses shows immunoreactivity over the postsynaptic plasma membrane (bold arrow opposite of T1, in D1) and in the nonsynaptic portion of the plasma membrane (small arrow). The immunoreactive dendrite almost envelops the axon terminal. The open arrow in another dendrite, D2, points to an unlabeled postsynaptic membrane with thin postsynaptic density. T1 and T2 = unlabeled terminals. B: The immunoreactive dendrite, D, from PND 4 tissue shows highly irregular contours (e.g. curved arrow), no apparent cytoskeleton, but instead, immunoreactive smooth saccules (small arrows). The postsynaptic membrane is immunoreactive (bold arrow). C: By PND 14, immunoreactivity is concentrated over postsynaptic densities (arrowhead), although extrasynaptic plasma membrane is not devoid of immunoreactivity (small arrows), particularly within labeled spines such as this one (LS). D: By PND 14, immunoreactivity also occurs discretely along the plasma membrane of astrocytic process (small arrows in A). Scale bar = 500 nm.

fine radiating processes were nearly abolished by preadsorption of the antiserum by the synthetic peptide. Semiquantitative electron microscopy showed approximately 90% reduction in the areal density of βAR404-ir processes within adult visual cortex following preadsorption of the antiserum by the antigenic peptide.

Discussion

Methodological considerations

This study used the preembedding immunoperoxidase labeling procedure for electron microscopy because of its exceptional sensitivity in detecting antigenic sites and because of its compatibility with procedures helpful for ultrastructural preservation of neural tissue, such as postfixation by osmium tetroxide and uranyl acetate. To further optimize immunodetection, the ultrastructural analysis was limited to the most superficial portions of Vibratome sections where access of immunoreagents to antigenic sites would be maximal. With this approach, immunoreactivity at postsynaptic membranes, as well as at unexpected sites, such as presynaptic terminals and membranes of fine astrocytic processes, was unambiguously detected. On the other hand, the approach has well-known limitations associated with diffusion of immunoperoxidase reaction products (Sternberger, 1986). For example, since diffusion of immunoperoxidase reaction products within cytosol is possible, we cannot be sure that the antigenic sites include membranes of

https://doi.org/10.1017/S0952523800011822 Published online by Cambridge University Press

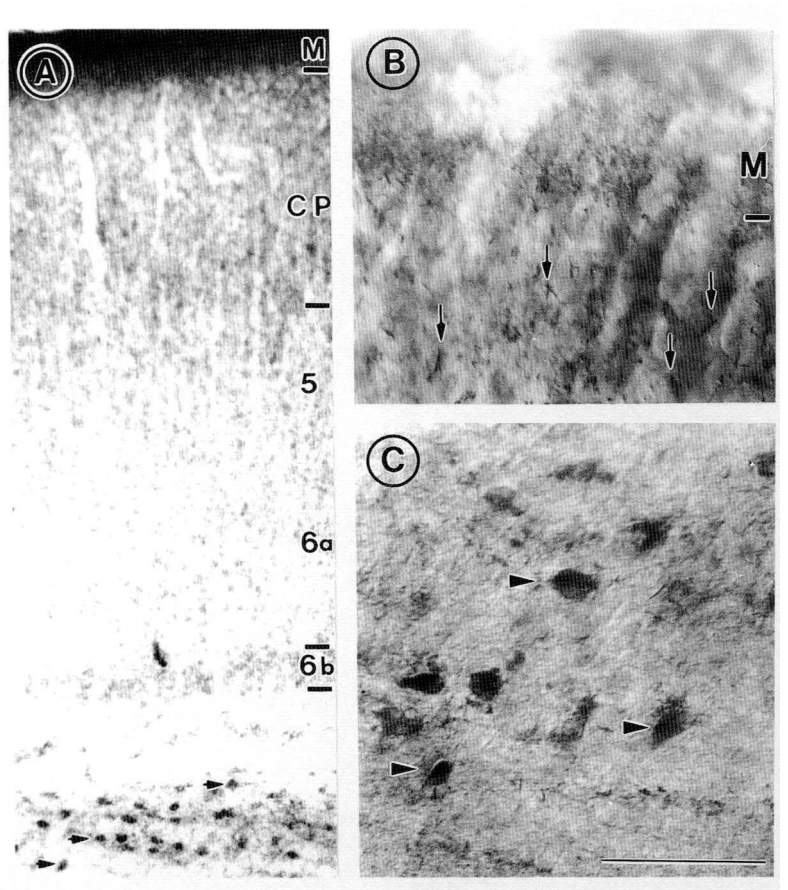

Fig. 4. βAR404-ir at PND 2. A: Immunoreactivity is most intense in the two extreme layers, i.e. the marginal zone and the white matter (ventral to layer 6b). B: A higher magnification micrograph of the marginal zone (future layer 1) reveals that immunoreactivity in this layer occurs as numerous puncta. The upper most tier of the cortical plate contains fine short processes (small arrows) and diffuse neuropilar staining. C: A light micrograph taken at a higher magnification shows that the intensely labeled perikarya in the white matter (arrowheads in panels A and C) are unaccompanied by labeling in processes. Scale bar = 200 μm in A, 50 μm in B and C.

intracellular organelles, such as vesicles and endoplasmic reticulum, that appear labeled when adjacent to immunoreactive plasma membranes.

βAR248 and βAR404 recognize different populations of cells

The predominant immunodetection of neurons by the third intracellular loop antiserum, βAR248, is consistent with previous findings using another monoclonal antibody (Aoki et al., 1989), also directed against the third intracellular loop portion of βAR. The astrocytic localization of antigen using the C-terminus antiserum, βAR404, also is not surprising in light of the previous observations that other monoclonal and polyclonal antibodies directed against the whole βAR molecule recognize neuronal and astrocytic processes (Aoki et al., 1987; Liu et al., 1993). Moreover, we had seen astrocytic labeling in adult rat and cat brain tissue previously using the βAR404 antiserum (Aoki, 1992; Aoki & Pickel, 1992). These observations suggest qualitative and quantitative differences in the neuronal versus astrocytic βAR, particularly in regards to the molecule's conformation.

Both the C-terminus and the third intracellular loop domains can be phosphorylated and this, in turn, alters the receptor's association with other intracellular molecules. β-arrestin is one such molecule known to bind to phosphorylated C-terminus (Yu et al., 1993). G_s proteins also interact with the receptor but at the third intracellular loop (Bouvier et al., 1988). Association by these molecules may render the antigenic domains more or less immunoreactive to the antisera. Experiments that correlate immunoreactivity with posttranslational modifications of βAR would be necessary to determine which, if any, of the above events occur during development. Even without results from such experiments, there is an undeniable increase in astrocytic βAR. On the other hand, results from such experiments would be helpful in determining whether the decline in βAR248-ir or of the unchanging concentration of βAR404-ir at morphologically identifiable synaptic junctions during postnatal development reflect a decline in the concentration of neuronal βAR or of conformational changes in neuronal βAR resulting in lowered antigenicity there.

The laminar distribution of βAR-ir differs from radioligand binding data

According to receptor autoradiography results, βAR density in adult rat cortices is highest in the supragranular layers, moderate in the infragranular layers, and minimal in layer 4 (Rainbow et al., 1984; Aoki et al., 1986; Schliebs & Godicke, 1988). The current immunocytochemical approach has provided information that complements, rather than overlap, with receptor autoradiography results. Immunoreactivity within neuronal and astrocytic perikarya is more evenly distributed across the layers but with additional intense immunoreactivity within layer 1 neuropil. This difference most likely arises because the antisera recognize not only those receptors that are ligand-binding (and thus detectable by receptor autoradiography), but also those in perikaryal cytoplasm that are undergoing desensitization, sequestration, *de novo* synthesis, or proteolysis (Strader et al., 1987*a*,*b*; Zemcik & Strader, 1988) and, thus, may not be as easily detected by receptor autoradiography. In support of the idea that the two antisera recognize receptors un-

https://doi.org/10.1017/S0952523800011822 Published online by Cambridge University Press

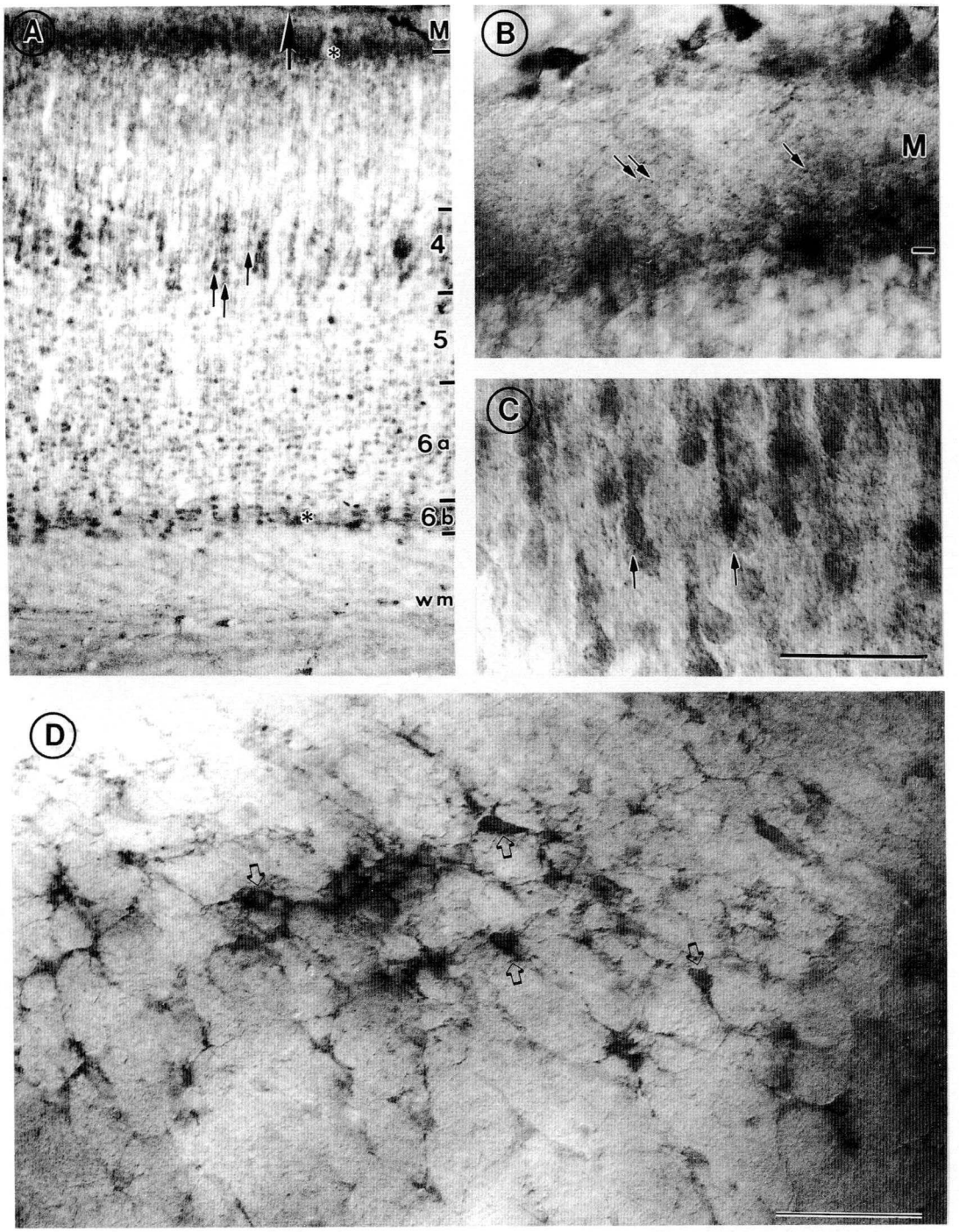

Fig. 5. βAR404-ir at PND 4. A: At this age, layer 4 has emerged as a layer distinct from the future layers 2/3. Immunoreactivity predominates in the newly formed layer 4, where individual perikarya and apical dendrites are evident (e.g. three small arrows). Bands of immunoreactivity are present at the base of the marginal zone (upper asterisk) and in layer 6b (lower asterisk). Intensely immunoreactive perikarya persist in layers 5 and 6a. wm = white matter. Large arrow points to pial surface. B: A light micrograph taken at a higher magnification shows that small immunoreactive puncta in the marginal zone (future layer 1) persist. C: In layer 4, the immunoreactivity is prominent within perikarya and processes projecting towards pial surface. The immunolabeled perikarya and processes exhibit a fine granular texture. D: Immunoreactivity in the white matter consists of fine branching processes that emerge radially from labeled perikarya. Scale bar = 200 μm in A, 50 μm in B–D.

dergoing turnover, immunoreactivity associated with membranous organelles involved in the turnover of plasma membrane proteins, such as the endocytotic and exocytotic vesicles and clear saccules very near postsynaptic membranes, frequently are immunoreactive.

βAR is scarce in the cortical plate

At PND 2, layers 2 through 4 are still very immature, and thus, are referred to as the cortical plate (Kageyama & Robertson, 1993).

https://doi.org/10.1017/S0952523800011822 Published online by Cambridge University Press

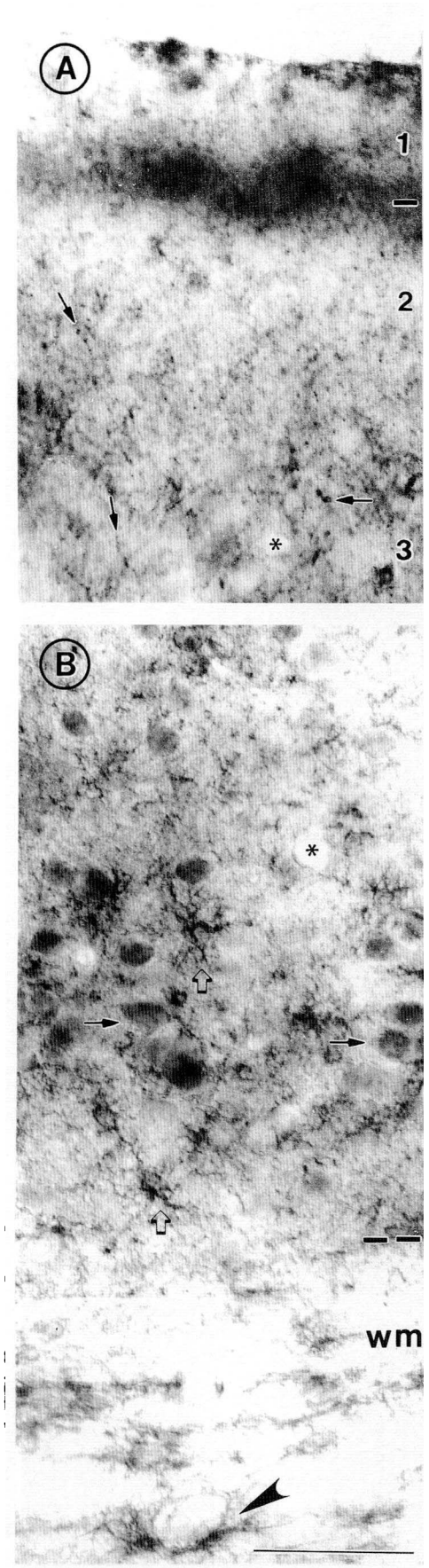

The present electron-microscopic observations confirm this, for the cortical plate is largely devoid of neuropil. Instead, this layer consists of tightly packed perikarya, each with very thin perikaryal cytoplasm. By PND 4, layer 4 neurons begin to extend neurites, but neurons in the future layers 2 and 3 still are without neurites.

The emergence of βAR-ir parallels the temporal pattern of neurite extension, since the cortical plate, containing these immature neurons, is largely devoid of immunoreactivity, while neurons located in the deeper layers exhibit prominent apical and basal dendrites exhibiting βAR248- and βAR404-ir. Overall, the emergence of immunoreactivity for both the βAR248 and βAR404 follows the inside-out pattern of cortical histogenesis.

βAR occur at morphologically identifiable synapses and at apparently nonjunctional sites of mature and immature dendrites

Although the βAR248 and βAR404 recognize different populations of cells in adulthood, morphological details of dendritic sites detected by the two antisera are similar throughout the ages. Already by the first postnatal week and throughout the ages, both antisera clearly detect postsynaptic membranes associated with thick postsynaptic densities. The major developmental change is in the calibre of immunoreactive dendrites: with maturation, the large irregularly shaped dendritic growth cones are replaced by fine processes, including spines. Moreover, quantitative analysis indicates that nearly all of the βAR404-ir in dendrites become associated with synapses by week 3.

The asymmetric morphology of immunoreactive synapses is consistent with previous reports stating that noradrenergic terminals form asymmetric synapses within the cerebral cortex (Olschowka et al., 1981; Parnavelas et al., 1985; Papadopoulos et al., 1987, 1989). However, based on an earlier study that labeled βAR simultaneously with a marker for catecholaminergic terminals (Aoki, 1992), it is also quite possible that the presynaptic elements at these junctional βAR-ir sites are not noradrenergic. Such cases are likely to reflect βAR-mediated postsynaptic modulation of glutamatergic synaptic transmission. Our results are consistent with the reports of Descarries et al. (Descarries et al., 1977; Séguéla et al., 1990) who have demonstrated that a majority of cortical noradrenergic terminals do not form morphologically junctional differentiated synapses, at least in the adult. Indeed, βAR-ir usually extends to apparently nonsynaptic portions of the plasma membrane within spines, and also occurs in large dendrites that lack morphologically identifiable synaptic inputs.

Thus, βAR-ir most likely reflects sites of noradrenergic modulation, responding to noradrenaline released at sites lacking morphologically identifiable synaptic features.

Synaptic βAR is most prevalent perinatally

The large portion of synaptic βAR sites detected during the first week (about 50%), compared to the third week (<5%), indicates

Fig. 6. βAR404-ir at PND 14. The intense band of immunoreactivity at the boundary between layers 1 and 2, first noted at PND 4, persists. A: βAR404-immunolabeling pattern is punctate (arrows). Immunolabeled neuronal perikarya, clearly visible at PND 4, are no longer resolvable. B: βAR404-immunolabeling pattern is distributed within fine radiating processes of astrocytes (clear arrows) in the vicinity of diffusely labeled neuronal perikarya (small arrows). In the white matter (wm), immunoreactive glial processes form rings around blood vessels (arrowhead). Asterisks: blood vessel lumens. Scale bar =50 μm in A and B.

https://doi.org/10.1017/S0952523800011822 Published online by Cambridge University Press

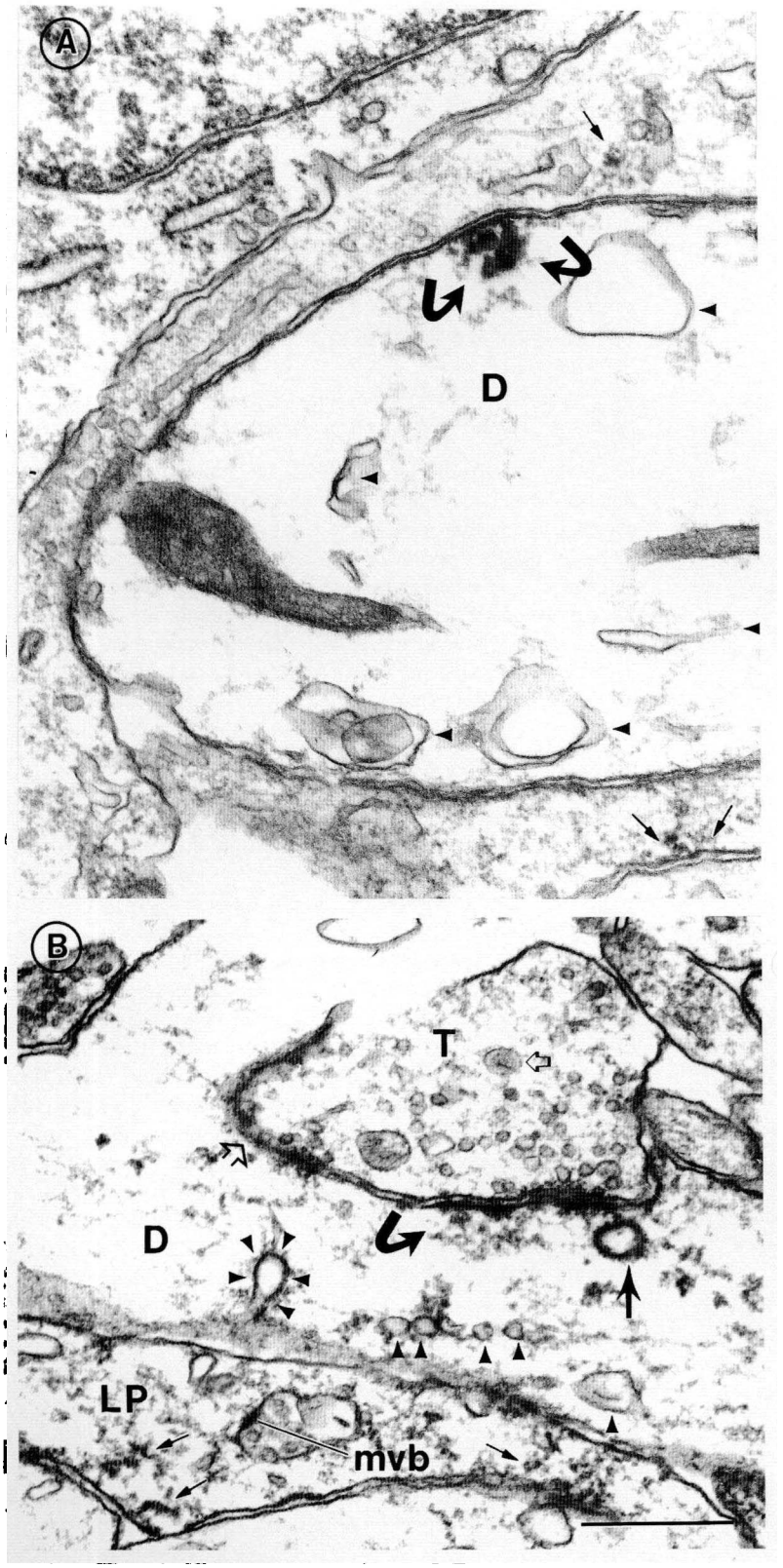

Fig. 7. βAR404-ir in immature neurites of PND 4 marginal zone as visualized by electron microscopy. A: A large-caliber dendritic growth cone (D) contains numerous saccules of the endoplasmic reticulum (arrowheads), indicating robust membrane turnover. βAR404-ir is evident along a patch of nonsynaptic plasma membrane (curved arrows). Other processes above and below D exhibit lighter immunoreactivity (small arrows). B: A dendritic shaft (D) exhibits immunoreactivity specifically at the synaptic junction. Curved arrow: immunolabeled portion of the postsynaptic membrane; open arrow: unlabeled portion of the postsynaptic density. Straight arrow: immunolabeled saccule near the labeled plasma membrane. Arrowheads: endocytotic saccules which are numerous in this and other immature dendrites. A group of five arrowheads points to a saccule that has fused with the plasma membrane. The unlabeled presynaptic terminal (T) contains a mixture of small clear vesicles and a dense-cored vesicle (clear arrow). The vesicles are clustered more heavily near the labeled synaptic specialization. Another labeled profile (LP) courses in the immediate vicinity. This profile exhibits diffuse immunoreactivity near the plasma membrane (small arrows) and associated with the multivesicular body (mvb). Scale bar = 500 nm.

that, relative to the other neurotransmitters affecting the visual cortex, noradrenaline has a much more dominant role in modulating synaptic transmission neonatally. Since the animal's eyes are still closed for most of this period, noradrenaline might be modulating synaptic transmission evoked by spontaneous firing of retinal ganglion cells. Although spontaneous firing may not be sufficient for solidifying binocular connections, this form of activity has been postulated to play a role in forming a rough organization of the cortex, such as the cortical columns in the visual cortex of prenatal primates (Horton & Hocking, 1996). Prior to PND 12,

https://doi.org/10.1017/S0952523800011822 Published online by Cambridge University Press

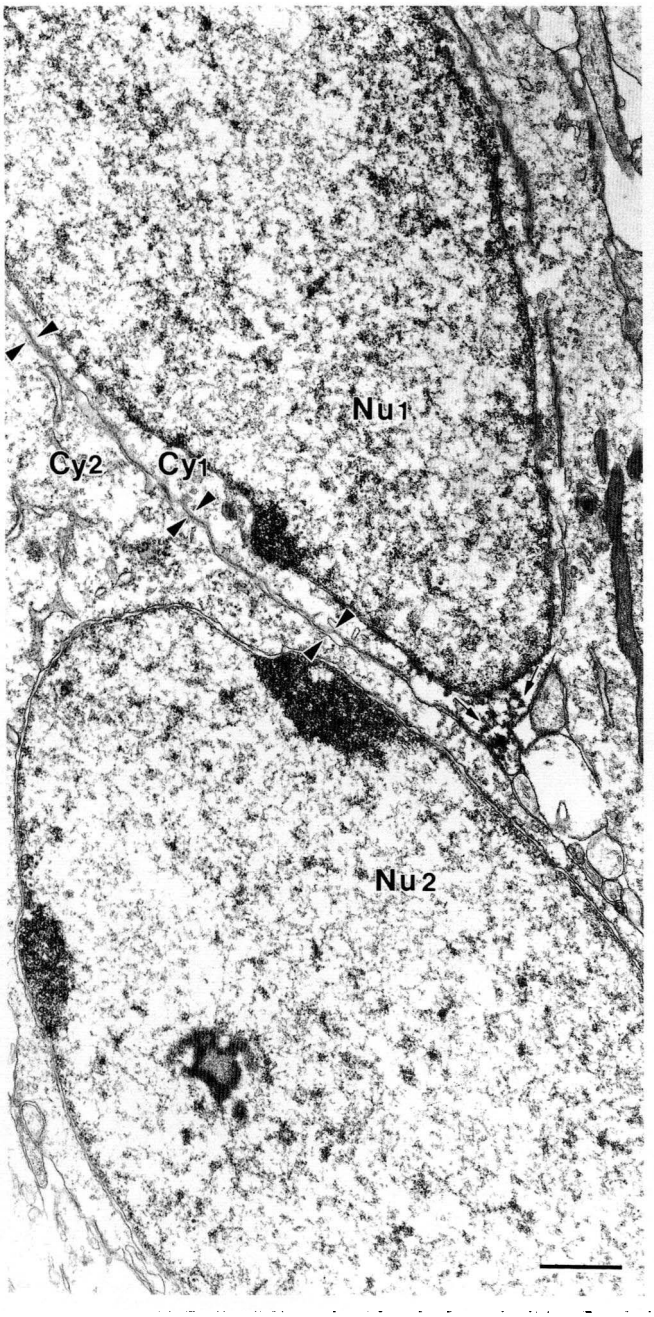

Fig. 8. βAR404-ir within the cortical plate of PND 4 tissue is scarce. Immunoreactivity is restricted to nonsynaptic portion of the plasma membrane (small arrows) of neuron 1, showing nucleoplasm and scarce cytoplasm (Nu1 and Cy1) within the plane of section. Arrowhead pairs point to direct juxtapositions of plasma membranes of neuron 1 and 2. Scale bar = 1 μm.

locus coeruleus neurons, from which noradrenergic fibers originate, are not responsive to visual stimuli (Nakamura et al., 1987). Thus, release of noradrenaline into the visual cortex probably is independent of visually evoked firing of locus coeruleus neurons. Noradrenaline release may be evoked by nonvisual or spontaneous firing of the locus coeruleus or be regulated by local cues within cortical neuropil arising from axo-axonic interactions (Fink et al., 1990; Wang et al., 1992; Lehmann et al., 1992; Andrés et al., 1993).

βAR occur in axons

Both βAR248 and βAR404 detect axonal processes. βAR404-ir axonal processes appear as early as PND 4 and persist at a similar areal density through PND 14. The presence of large clusters of vesicles within these immunoreactive axons suggest that these profiles are capable of neurotransmitter release even if not at morphologically identifiable synaptic junctions. The immunoreactive axons form both symmetric and asymmetric synaptic junctions which, in turn, have been correlated with inhibitory and excitatory synaptic transmission, respectively (Gray, 1959). Thus, these immunoreactive axons may reflect sites where release of inhibitory and excitatory neurotransmitters is regulated *via* axo-axonic interactions with noradrenergic terminals. Alternatively, βAR on axons may reflect autoreceptors. As of yet, there is no evidence for βAR-mediated regulation of noradrenaline release (Chesselet, 1984). Perhaps βAR activation regulates a cellular event other than transmitter release, such as motility of axonal growth cones.

Astrocytic βAR undergo dramatic postnatal increase

Already by PND 4, astrocytic perikarya are immunoreactive to βAR404 within the white matter. In contrast to neuronal labeling, which is remarkably constant throughout development, the areal density of astrocytic labeling in the grey matter undergoes a 200-fold increase from the first to the third week, thereby becoming the dominant immunoreactive profile in adulthood. One explanation for this dramatic increase in astrocytic immunolabeling is the increase in density of astrocytes (Ling & Leblond, 1973; Parnavelas et al., 1983). This dramatic shift in the distribution pattern of βAR404-ir profiles during the first postnatal month indicates that noradrenergic action within neonatal cortices transforms from modulation of synaptic transmission during the first week to a more spatially and temporally diffuse modulation involving activation of multiple astrocytic processes.

Functional significance of neuronal and astrocytic βAR in developing visual cortices

This study was originally motivated by reports indicating that βAR activation is required for early postnatal experience to cause lifelong alternations in cortical circuitry, as assayed by ocular dominance shift following monocular deprivation of cats (Kasamatsu, 1991). As expected, βAR are not the only agents dictating visual cortical plasticity: it has since been shown that muscarinic type of cholinergic receptors, NMDA-type glutamate receptors and neurotrophic factors also are involved in determining the degree of cortical plasticity (Bear & Singer, 1986; Gordon et al., 1990; review by Rauschecker, 1991; Maffei et al., 1992; Domenici et al., 1992; Fagiolini et al., 1994). Nevertheless, the later works also support the original findings of Kasamatsu et al. regarding βAR participation in developmental plasticity.

βAR is coupled positively to adenylyl cyclase. Thus, activation of this receptor leads to a rise in intracellular cyclic AMP (cAMP). As for the βAR-mediated neuronal responses, receptive-field properties of visual cortical neurons are better tuned during iontophoretic application of noradrenaline (Waterhouse et al., 1990). This may be because βAR activation reduces spike-frequency accommodation (Madison & Nicoll, 1986) while also potentiating $GABA_A$-receptor-induced changes in membrane conductance (Waterhouse et al., 1990), and reduced uptake of L-glutamate into astrocytes (Hansson, 1992) leading to increased levels of L-glutamate at the synaptic cleft.

https://doi.org/10.1017/S0952523800011822 Published online by Cambridge University Press

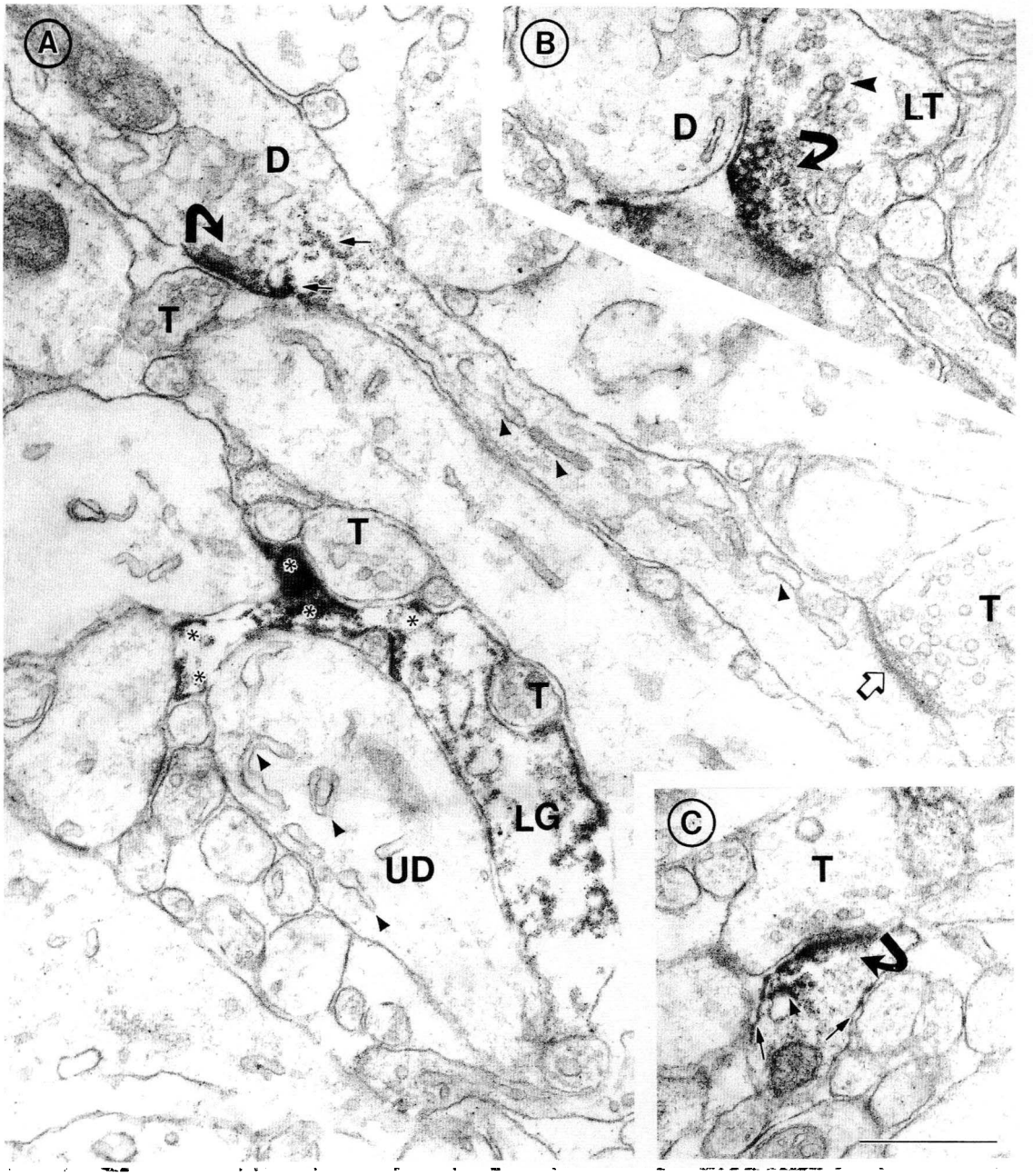

Fig. 9. By PND 10, βAR404-ir is in dendritic shafts, spines, and astrocytes. A: A dendritic shaft in layer 2 exhibits two synaptic junctions, one labeled (upper curved arrow) and another unlabeled (lower clear arrow). Immunoreactivity also occurs in the same dendrite's cytoplasm near the immunoreactive synapse (small arrows). This and another unlabeled dendritic profile (UD), both, contain many saccules of the endoplasmic reticulum (arrowheads), indicating active turnover of the plasma membrane. T: presynaptic terminals, unlabeled. Another profile exhibits intense immunoreactivity along the plasma membrane. Judging by its irregular contour (asterisks), this is a glial profile (LG), most likely of an astrocyte. B: A terminal containing a mixture of small clear vesicles and a large dense-cored vesicle (arrowhead) is immunolabeled (curved arrow in LT). Immunoreactivity is associated with vesicular and plasma membranes. LT forms a symmetric synaptic junction with a dendrite (D). C: A small dendritic spine also is immunoreactive. Note the association of immunoreactivity with the postsynaptic membrane (curved arrow), small saccule (arrowhead) and extrasynaptic plasma membrane (small arrows). Scale bar = 500 nm.

One major effect following stimulation of astrocytic βAR is glycogenolysis (review by Stone & Ariano, 1989). Noradrenaline would be released in the visual cortex as the animal is brought to a vigilant or aroused state (Aston-Jones et al., 1991). Thus, astrocytic βAR may provide ATP and metabolic substrates to match cortical neuropil's enhanced activity, as the animal is brought to an aroused state by nonvisual stimuli prior to eye opening and by visual stimuli throughout and beyond the critical period for developmental plasticity.

βAR activation leads to the formation of processes by astrocytes, perhaps as actin depolymerizes intracellularly, thereby allowing reorganization of the cytoskeletal matrix (Goldman &

https://doi.org/10.1017/S0952523800011822 Published online by Cambridge University Press

Table 1. *Areal density (Areal D) of βAR404-ir profiles in layer 1 of developing rat visual cortex according to postnatal age*[a]

	Age		
Immunoreactive site	1 Week (4660 μm^2; 0.43)	2 Weeks (10720 μm^2; 6.42)	3 Weeks (10250 μm^2; 12.96)
Dendritic	0.32	0.42	0.37
Postsynaptic	0.23	0.32	0.37
Axonal	0.19	0.22	0.10
Presynaptic	0.04	0.07	0.37
Glial	0.04	1.85	8.46

[a]Tissue was obtained from 1 week (PND 4 and PND 7), 2 weeks (PND 10, PND 13, and PND 14), and 3 weeks postnatal (PND 24) rat visual cortex. The total surveyed area and the areal density of synapses for each group is indicated in parentheses. The areal density of profiles exhibiting immunoreactive sites is expressed in the units, "encountered per 100 μm^2." The areal density of immunoreactive sites that occurred postsynaptically within dendrites are shown in the row, "Postsynaptic," while those that occurred presynaptically within axons are shown in the row, "Presynaptic."

Abramson, 1990). In the hypothalamus, this leads to increased neuronal contact with the basal lamina of blood vessels (Bicknell et al., 1989; Smithson et al., 1990). Perhaps in the cerebral cortex, noradrenaline causes retraction of astrocytic processes residing between fine neuronal processes, thereby regulating the degree of axo-axonic and axo-dendritic interactions that take part in cortical synaptic circuitry.

βAR-dependent cAMP production within astrocytes leads to the release of nerve growth factor (NGF) (Schwartz, 1988). NGF, in turn, promotes formation of binocular connections and of their functional recovery following monocular deprivation (Carmignoto et al., 1993; Berardi et al., 1994). Thus, it is conceivable that βAR-dependent synthesis and release of neurotrophic factors from astrocytes facilitate the formation of functional cortical circuitry in the visual cortex in ways that mirror experience during early life. In light of the finding that exogenous supplies of cultured astrocytes can reinstate ocular dominance plasticity in adult cat visual cortices (Müller & Best 1989), it would be interesting to learn whether these transplanted astrocytes exhibit any of the above βAR-mediated responses.

Acknowledgments

This work was funded by the following grants to C. Aoki: NIH-NINDS NS30944, NIH-NEI EY08055, NSF RCD92-53750 (Presidential Faculty Fellowship), and Human Frontiers Science Program Award RG-16/93. Thanks to Dr. Alev Erisir for reading the manuscript; Charu Venkatesan, C.-G. Go, X.-Z. Song, Zak Shusterman, Alice Elste, and Dr. Susan Lee for their technical support; and Mian Hou for photographic reproductions.

References

ANDRÉS, M.E., BUSTOS, G. & GYSLING, K. (1993). Regulation of [^{3}H]norepinephrine release by N-methyl-D-aspartate receptors in minislices from the dentate gyrus and the CA1-CA3 area of the rat hippocampus. *Biochemical Pharmacology* **46**, 1983–1987.

AOKI, C. (1992). β-adrenergic receptors: Astrocytic localization in the adult visual cortex and their relation to catecholamine axon terminals as revealed by electron microscopic immunocytochemistry. *Journal of Neuroscience* **12**, 781–792.

AOKI, C. & PICKEL, V.M. (1992). C-terminal tail of β-adrenergic receptors: Immunocytochemical localization within astrocytes and their relation to catecholaminergic neurons in N. tractus solitarii and area postrema. *Brain Research* **571**, 35–49.

AOKI, C. & VENKATESAN, C. (1994). An antibody directed against the C-terminal tail of β-adrenergic receptor recognizes astrocytes in adult brain but neurons neonatally. *Society for Neuroscience Abstracts* **20**, 877.

AOKI, C., KAUFMAN, D. & RAINBOW, T.C. (1986). The ontogeny of the laminar distribution of β-adrenergic receptors in the visual cortex of cats, normally reared and visually deprived. *Developmental Brain Research* **27**, 109–116.

AOKI, C., JOH, T.H. & PICKEL, V.M. (1987). Ultrastructural localization of β-adrenergic receptor-like immunoreactivity in the cortex and neostriatum of rat brain. *Brain Research* **437**, 264–282.

AOKI, C., ZEMCIK, B.A., STRADER, C.D. & PICKEL, V.M. (1989). Cytoplasmic loop of β-adrenergic receptors: Synaptic and intracellular localization and relation to catecholaminergic neurons in the nuclei of the solitary tracts. *Brain Research* **493**, 331–347.

AOKI, C., VENKATESAN, C., GO, C.-G., MONG, J.A. & DAWSON, T.M. (1994). Cellular and subcellular localization of NMDA-R1 subunit immunoreactivity in the visual cortex of adult and neonatal rats. *Journal of Neuroscience* **14**, 5202–5222.

ASTON-JONES, G., CHIANG, C. & ALEXINSKY, T. (1991). Discharge of noradrenergic locus coeruleus neurons in behaving rats and monkeys suggests a role in vigilance. *Progress in Brain Research* **88**, 501–519.

BEAR, M.F. & SINGER, W. (1986). Modulation of visual cortical plasticity by acetylcholine and noradrenaline. *Nature* **320**, 172–176.

BERARDI, N., CELLERINO, A., DOMENICI, L., FAGIOLINI, M., PIZZORUSSO, T., CATTANEO, A. & MAFFEI, L. (1994). Monoclonal antibodies to nerve growth factor affect the postnatal development of the visual system. *Proceedings of the National Academy of Sciences of the U.S.A.* **91**, 684–688.

BICKNELL, R.J., LUCKMAN, S.M., INENAGA, K., MASON, W.T. & HATTON, G.I. (1989). Beta-adrenergic and opioid receptors on pituicytes cultured from adult rat neurohypophysis: Regulation of cell morphology. *Brain Research Bulletin* **22**, 379–388.

BLUE, M.E. & PARNAVELAS, J.G. (1983*a*). The formation and maturation of synapses in the visual cortex of the rat. I. Qualitative analysis. *Journal of Neurocytology* **12**, 599–616.

BLUE, M.E. & PARNAVELAS, J.G. (1983*b*). The formation and maturation of synapses in the visual cortex of the rat. II. Quantitative analysis. *Journal of Neurocytology* **12**, 697–712.

BOUVIER, M., HAUSDORFF, W.P., DE BLASI, A., O'DOWD, B.F., KOBILKA, B.K., CARON, M.G. & LEFKOWITZ, R.J. (1988). Removal of phosphorylation sites from the β2-adrenergic receptor delays onset of agonist-promoted desensitization. *Nature* **333**, 370–373.

CARMIGNOTO, G., CANELLA, R., CANDEO, P, COMELLI, M.C. & MAFFEI, L. (1993). Effects of nerve growth factor on neuronal plasticity of the kitten visual cortex. *Journal of Physiology* **464**, 343–360.

CHESSELET, M.-F. (1984). Presynaptic regulation of neurotransmitter release in the brain. *Neuroscience* **12**, 347–375.

COYLE, J.T. & MOLLIVER, M.E. (1977). Major innervation of newborn rat cortex by monoaminergic neurons. *Science* **196**, 444–447.

CRAGG, B.G. (1975). The development of synapses in kitten visual cortex during visual deprivation. *Experimental Neurology* **46**, 445–451.

DESCARRIES, L., WATKINS, K.C. & LAPIERRE, Y. (1977). Noradrenergic axon terminals in the cerebral cortex of rat. III. Topometric ultrastructural analysis. *Brain Research* **133**, 197–222.

DIXON, R.A., KOBILKA, B.K., STRADER, D.J., BENOVIC, J.L., DOHLMAN, H.G., FRIELLE, T., BOLANOWSKI, M.A., BENNETT, C.D., RANDS, E., DIEHL, R.E., MUMFORD, R.A., SLATER, E.E., SIGAL, I.S., CARON, M.G., LEFKOWITZ, R.J. & STRADER, C.D. (1986). Cloning of the gene and cDNA for mammalian β-adrenergic receptor and homology with rhodopsin. *Nature* **321**, 75–79.

DOMENICI, L., PARISI, V. & MAFFEI, L. (1992). Exogenous supply of nerve growth factor prevents the effects of strabismus in the rat. *Neuroscience* **51**, 19–24.

FAGIOLINI, M., PIZZORUSSO, T., BERARDI, N., DOMENICI, L. & MAFFEI, L. (1994). Functional postnatal development of the rat primary visual cortex and the role of visual experience: Dark rearing and monocular deprivation. *Vision Research* **34**, 709–720.

FINK, K., BÖNISCH, H. & GÖTHERT, M. (1990). Presynaptic NMDA receptors stimulate noradrenaline release in the cerebral cortex. *European Journal of Pharmacology* **185**, 115–117.

GOLDMAN, J.E. & ABRAMSON, B. (1990). Cyclic AMP-induced shape changes of astrocytes are accompanied by rapid depolymerization of actin. *Brain Research* **528**, 189–196.

GORDON, B., MITCHELL, B., MOHTADI, K., ROTH, E., TSENG, Y. & TURK, F. (1990). Lesion of nonvisual inputs affect plasticity, norepinephrine content, and acetylcholine content of visual cortex. *Journal of Neurophysiology* **64**, 1851–1860.

GRAY, E.G. (1959). Axo-somatic and axo-dendritic synapses of the cerebral cortex. *Journal of Anatomy* **93**, 420–433.

HANSSON, E.A. (1992). Adrenergic receptor regulation of amino acid neurotransmitter uptake in astrocytes. *Brain Research Bulletin* **29**, 297–301.

HORTON, J.C. & HOCKING, D.R. (1996). An adult-like pattern of ocular dominance columns in striate cortex of newborn monkeys prior to visual experience. *Journal of Neuroscience* **16**, 1791–1807.

HSU, S.M., RAINE, L. & FANGER, H. (1981). Use of avidin-biotin-peroxidase complex (ABC) in immunoperoxidase techniques: A comparison between ABC and unlabeled antibody (PAP) procedures. *Journal of Histochemistry and Cytochemistry* **21**, 312–332.

KAGEYAMA, G.H. & ROBERTSON, R.T. (1993). Development of geniculocortical projections to visual cortex in rat: Evidence for early ingrowth and synaptogenesis. *Journal of Comparative Neurology* **335**, 123–148.

KASAMATSU, T. (1991). Adrenergic regulation of visuocortical plasticity: A role of the locus coeruleus system. *Progress in Brain Research* **88**, 599–616.

KING, J.C., LECHAN, R.M., KUIGEL, G. & ANTHONY, E.L.P. (1983). Acrolein: A fixative for immunocytochemical localization of peptides in the central nervous system. *Journal of Histochemistry and Cytochemistry* **31**, 62–68.

LEHMANN, J., VALENTINO, R. & ROBINE, V. (1992). Cortical norepinephrine release elicited *in situ* by N-methyl-D-aspartate (NMDA) receptor stimulation: A microdialysis study. *Brain Research* **599**, 171–174.

LEVITT, P. & MOORE, R.Y. (1979). Development of the noradrenergic innervation of neocortex. *Brain Research* **162**, 243–259.

LING, E.A. & LEBLOND, C.P. (1973). Investigation of glial cells in semithin sections. II. Variations with age in the numbers of the various glial cell types in rat cortex and corpus callosum. *Journal of Comparative Neurology* **149**, 73–82.

LIU, Y., JIA, W., STROSBERG, A.D. & CYNADER, M. (1993). Development and regulation of β-adrenergic receptors in kitten visual cortex: An immunocytochemical and autoradiographic study. *Brain Research* **632**, 274–286.

MADISON, D.V. & NICOLL, R.A. (1986). Actions of noradrenalin recorded intracellularly in rat hippocampal CA1 pyramidal neurons, *in vitro*. *Journal of Physiology* **372**, 221–244.

MAFFEI, L., BERARDI, N., DOMENICI, L., PARISI, V. & PIZZORUSSO, T. (1992). Nerve growth factor (NGF) prevents the shift in ocular dominance distribution of visual cortical neurons in monocularly deprived rats. *Journal of Neuroscience* **12**, 4651–4662.

MOLLIVER, M.E. & KRISTT, D.A. (1975). The fine structural demonstration of monoaminergic synapses in immature rat neocortex. *Neuroscience Letters* **1**, 305–310.

MORRISON, J.H., GRZANNA, R., MOLLIVER, M.E. & COYLE, J.T. (1978). The distribution and orientation of noradrenergic fibers in neocortex of the rat: An immunofluorescence study. *Journal of Comparative Neurology* **181**,17–40.

MÜLLER, C.M. & BEST, J. (1989). Ocular dominance plasticity in adult cat visual cortex after transplantation of cultured astrocytes. *Nature* **342**, 427–430.

NAKAMURA, S., KIMURA, F. & SAKAGUCHI, T. (1987). Postnatal development of electrical activity in the locus coeruleus. *Journal of Neurophysiology* **58**, 510–524.

OLSCHOWKA, J.A., MOLLIVER, M.E., GRZANNA, R., RICE, F.L. & COYLE, J.T. (1981). Ultrastructural demonstration of noradrenergic synapses in the rat central nervous system by dopamine-beta-hydroxylase immunocytochemistry. *Journal of Histochemistry and Cytochemistry* **29**, 271–280.

PAPADOPOULOS, G.C., PARNAVELAS, J.G. & BUIJS, R.M. (1987). Monoaminergic fibers form conventional synapses in the cerebral cortex. *Neuroscience Letters* **7**, 275–279.

PAPADOPOULOS, G.C., PARNAVELAS, J.G. & BUIJS, R.M. (1989). Light and electron microscopic immunocytochemical analysis of the noradrenaline innervation of the rat visual cortex. *Journal of Neurocytology* **18**, 1–10.

PARNAVELAS, J.G., LUDER, R., POLLARD, S.G., SULLIVAN, K. & LIEBERMAN, A.R. (1983). A qualitative and quantitative ultrastructural study of glial cells in the developing visual cortex of the rat. *Philosophical Transactions of the Royal Society B* (London) **301**, 55–84.

PARNAVELAS, J.G., MOISES, H.C. & SPECIALE, S.G. (1985). The monoaminergic innervation of the rat visual cortex. *Proceedings of the Royal Society B* (London) **223**, 319–329.

PETERS, A., PALAY, S.L. & WEBSTER, H. DEF. (1991). *The Fine Structure of the Nervous System*. New York: Oxford University Press.

RAINBOW, T.C., PARSONS, B. & WOLFE, B.B. (1984). Quantitative autoradiography of beta1- and beta2-adrenergic receptors in rat brain. *Proceedings of the National Academy of Sciences of the U.S.A.* **81**, 1585–1589.

RAUSCHECKER, J.P. (1991). Mechanisms of visual plasticity: Hebb synapses, NMDA receptors and beyond. *Physiological Reviews* **71**, 587–615.

SCHLIEBS, R. & GODICKE, C. (1988). Laminar distribution of noradrenergic markers in rat visual cortex. *Neurochemistry International* **13**, 481–486.

SCHWARTZ, J.P. (1988). Stimulation of nerve growth factor mRNA content in C6 glioma cells by β-adrenergic receptor and cAMP. *Glia* **1**, 282–285.

SÉGUÉLA, P., WATKINS, K.C., GEFFARD, M. & DESCARRIES, L. (1990). Noradrenaline axon terminals in adult rat neocortex: An immunocytochemical analysis in serial thin sections. *Neuroscience* **35**, 249–264.

SMITHSON, K.G., SUAREZ, I. & HATTON, G.I. (1990). β-adrenergic stimulation decreases glial and increases neural contact with the basal lamina in rat neurointermediate lobes incubated *in vitro*. *Journal of Neuroendocrinology* **2**, 693–699.

STERNBERGER, L.A. (1986). *Immunocytochemistry*, 3rd edition. New York: John Wiley.

STONE, E.A. & ARIANO, M.A. (1989). Are glial cells targets of the central noradrenergic system? A review of the evidence. *Brain Research Reviews* **14**, 297–309.

STRADER, C.D., SIGAL, I.S., REGISTER, R.B., CANDELORE, M.R., RANDS, E. & DIXON, R.A.F. (1987*a*). Identification of residues required for ligand binding to the β-adrenergic receptor. *Proceedings of the National Academy of Sciences of the U.S.A.* **84**, 4384–4388.

STRADER, C.D., SIGAL, I.S., BLAKE, A.D., CHEUNG, A.H., REGISTER, B.S., RANDS, E., ZEMCIK, B.A., CANDELORE, M.R. & DIXON, R.A.F. (1987*b*). The carboxyl terminus of the hamster β-adrenergic receptor expressed in mouse L cells is not required for receptor sequestration. *Cell* **49**, 855–863.

VENKATESAN, C., SONG, X-A., GO, C.-G., KUROSE, H. & AOKI, C. (1996). Cellular and subcellular distribution of α_{2A}-adrenergic receptors in the visual cortex of neonatal and adult rats. *Journal of Comparative Neurology* **365**, 79–95.

VOS, P, KAUFMANN, D., HAND, P.J. & WOLFE, B.B. (1990). β2-adrenergic receptors are colocalized and coregulated with "whisker barrels" in rat somatosensory cortex. *Proceedings of the National Academy of Sciences of the U.S.A.* **87**, 5114–5118.

WANG, J.K.T., ANDREWS, H. & THUKRAL, V. (1992). Presynaptic glutamate receptors regulate noradrenaline release from isolated nerve terminals. *Journal of Neurochemistry* **58**, 204–211.

WATERHOUSE, B.D., AZIZI, S.A., BURNE, R.A. & WOODWARD, D.J. (1990). Modulation of rat cortical area 17 neuronal responses to moving visual stimuli during norepinephrine and serotonin microiontophoresis. *Brain Research* **514**, 276–292.

WILKINSON, M., SHAW, C., KHAN, I. & CYNADER, M. (1983). Ontogenesis of β-adrenergic binding sites in kitten visual cortex and the effects of visual deprivation. *Developmental Brain Research* **7**, 349–352.

YU, S.S., LEFKOWITZ, R.J. & HAUSDORFF, W.P. (1993). β-Adrenergic receptor sequestration: A potential mechanism of receptor resensitization. *Journal of Biological Chemistry* **268**, 337–341.

ZEMCIK, B.A. & STRADER, C.D. (1988). Fluorescent localization of the β-adrenergic receptor on DDT-1 cells: Down-regulation by adrenergic agonists. *Biochemical Journal* **251**, 333–339.